Automatic Detection of Delamination on Tunnel Lining Surfaces from Laser 3D Point Cloud Data by 3D Features and Support Vector Machine

Tsukasa Mizutani[a], Takahiro Yamaguchi[a,*], Kazutomo Yamamoto[b], Tetsuya Ishida[c], Yoshifumi Nagata[d], Hinari Kawamura[e], Tomoaki Tokuno[e], Kiyoshi Suzuki[b], Yuya Yamaguchi[b]

[a] *Institute of Industrial Science, the University of Tokyo, 4-6-1, Komaba, Meguro-ku, Tokyo, 153-8505, Japan*

[b] *Aero Asahi Corporation, 3-14-4, Minamidai, Kawagoe, Saitama, 350-1165, Japan*

[c] *Department of Civil Engineering, the University of Tokyo, 7-3-1, Hongo, Bunkyo-ku, Tokyo, 113-8654, Japan*

[d] *Metropolitan Expressway Company Limited, 1-4-1, Kasumigaseki, Chiyoda-ku, Tokyo, 100-8930, Japan*

[e] *Shutoko Engineering Company Limited, 3-10-11, Toranomon, Minato-ku, Tokyo, 105-0001, Japan*

Abstract

A completely automatic and accurate detection algorithm for the delamination on tunnel concrete lining surfaces from laser 3D point cloud data is proposed. A Mobile Mapping System (MMS), which mounts laser sensors and a positioning system, is utilized to measure the geometry of tunnel lining surfaces highspeed. The proposed algorithm consists of 4 steps: removal of tunnel profile components, detection of peaks of anomalies, localization of anomaly areas, classification of delamination and appendages. On tunnel linings, there are many appendages such as cables, lights, signs, and water guides to mask the features of delamination. In the article, a novel 3D feature was introduced to realize the accurate classification. An automatic SVM algorithm was developed using real tunnel lining data and manual inspection results, showing an accurate delamination map.

Keywords: Mobile Mapping System (MMS); Delamination; Tunnel Linings; Laser 3D Point Cloud Data; Support Vector Machine (SVM)

1. Introduction

To maintain enormous amounts of aging infrastructure stocks, non-contact and highspeed monitoring techniques are indispensable [1]-[3]. One of the important social concerns is pop out of tunnel concrete linings, which threatens the safety of road users. To prevent severe accidents, road administrators need to detect delamination before it advances to peeling.

In practice, delamination of concrete structures is detected by a hammering test. The problem is it is labor-intensive. Covering huge areas of tunnel lining surfaces by manual inspection is not feasible. Furthermore, inspection results are subjective, demanding skilled inspectors to accurately detect damages. InfraRed (IR) camera method detects delamination by the difference of surface temperature [4]. It needs the difference of temperature between day and night. An automatic sounding system records acoustic signals [5]. A laser sounding system hits light to evaluate dynamic characteristics of delaminated concrete surfaces [6]. A non-destructive monitoring method inside concrete structures by neuron sources is being developed [7]. These methods need special instruments, inspection time and costs. Our research group is utilizing Ground Penetrating Radar (GPR) mounted on vehicles, though it is difficult in principle to detect millimeter order thickness cracks by the frequency range of typical commercialized measurement systems [8].

To solve the problem, a Mobile Mapping System (MMS) was utilized in the research. Ranging lasers and a GNSS/IMU positioning system are mounted on a ordinary MMS (Fig. 1) [9]. The advantages of an MMS are highspeed and a high-resolution grid data of altitude (height) of an infrastructure surface can be measured. As reported in our previous research works, when delamination advances to a certain extent, it causes at least a several tens centimeter area and several millimeter height deformations [10],[11]. Our claim is at that stage delamination is detected as a positive peak of a local displacement from laser 3D point cloud data.

In terms of the previous research about laser method, Kim *et al.* conducted the quality assessment of precast concrete. They estimated areas of spalling by an edge

* Corresponding author.

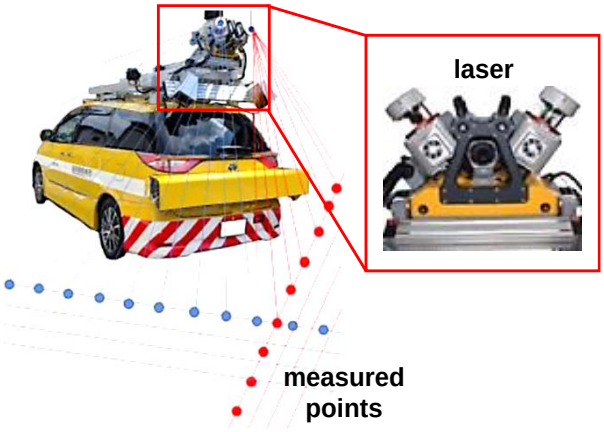

Fig. 1. Mobile mapping system (MMS) for obtaining laser 3D point cloud data.

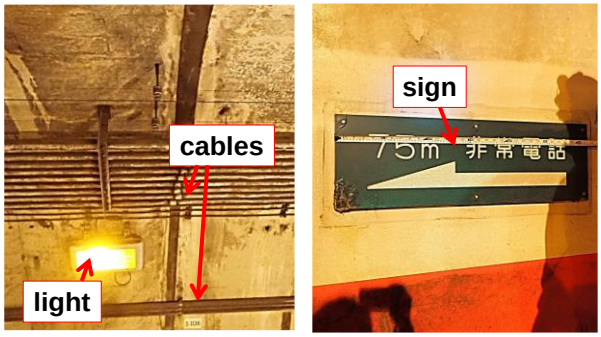

(a) (b)

Fig. 2. Appendages on real tunnel lining surfaces. (a) Cables and light. (b) Sign.

detection algorithm [12]. Yoon *et al.* illustrates utility cables on tunnel lining using laser data as a feasibility study [13]. Our group first proposed an automatic algorithm to detect delamination on concrete surfaces adopting signal and image processing approaches [10],[11]. The characteristic of the algorithm is the 3D geometries of anomalies are accurately extracted to calculate feature values, detecting delamination and showing their shapes on a 3D map.

The problem of the research [10]-[13] is, the environment of a real tunnel lining is complicated, including many appendages and ambiguous features such as cables, lights, signs, water guides and noises as shown in Fig. 2. There are at most several areas of delamination in a 100 m section. They are subtle in their nature, resulting in an unacceptable number of false detections. It is necessary to increase accuracy by adding feature values to discriminate artificial objects of appendages. The other problem is there were five parameters to threshold. It is arbitrary to decide the thresholding ranges of parameters and may not have generality when applied to other tunnel measurement data. Deep learning algorithms to classify delamination and appendages is straightforward though large training data, at least ten thousand to one hundred thousand features are needed [14]-[17] to conduct reliable training. The automatic estimation of classification criteria of parameters by simple machine learning method is necessary.

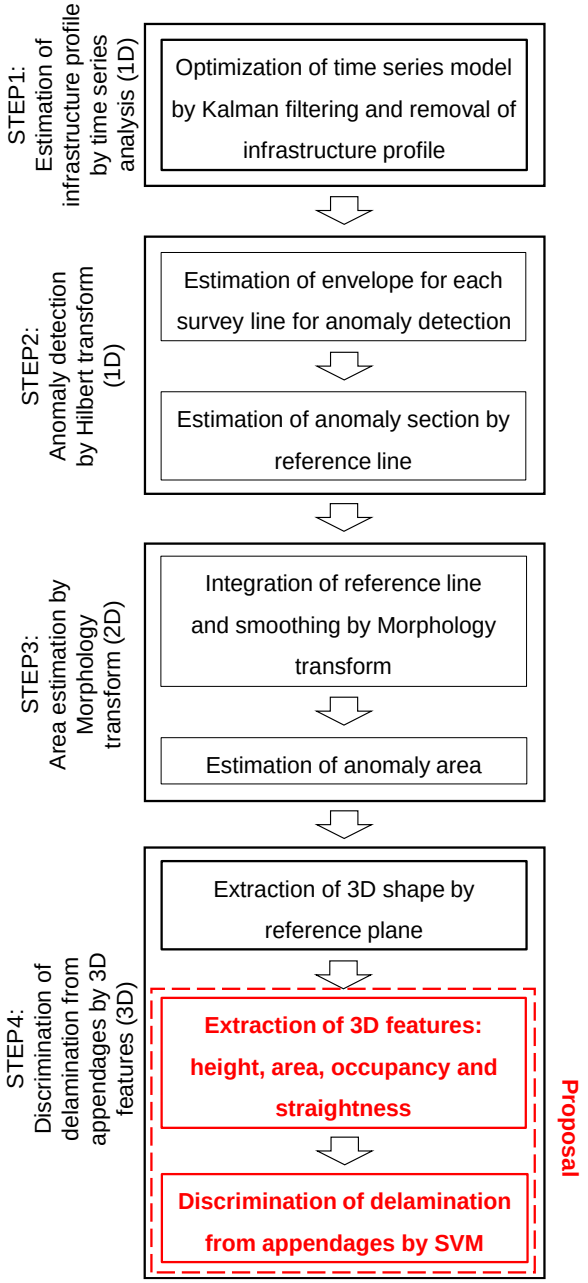

Fig. 3. Flowchart of the algorithm. The algorithm is based on [10], [11]. This research deals with the extraction of 3D features and automatic detection of delamination by SVM.

2. Contributions of the research

In response to the discussions above, the contributions of the research are summarized below.

1) To accurately detect delamination, besides maximum height, area and occupancy, the 'straightness' of an outline of a 3D object was defined by Hough transform to eliminate artificial objects of tunnel appendages. Straightness is a novel index in the context of pattern analysis research.

2) Support Vector Machine (SVM), one of the most typical and simple machine learning algorithms was trained by real tunnel measurement data to realize automatic detection.

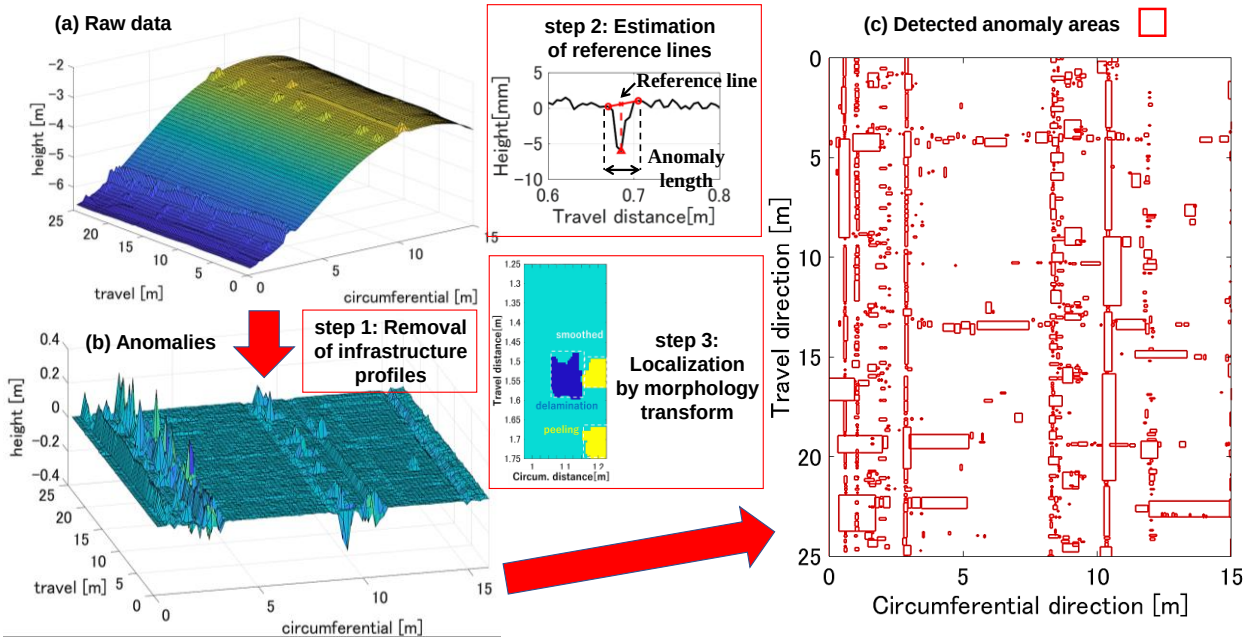

Fig. 4. Extraction of anomalies from laser measurement data [11]. (a) Raw tunnel lining data. (b) After removal of a tunnel profile. (c) Candidate anomaly areas. Corresponding step 1 to step 3 are also shown.

The rest of the paper is organized as follows: Section 3 introduces the concept of the algorithm of the previous research [10],[11] and proposal of this research; Section 4 describes the configuration of the utilized system and training and validation data; Section 5 proposes the novel 3D feature for automatic detection. Section 6 shows the detection result by SVM and discusses the optimized SVM model. Parametric studies were conducted showing constructed dividing planes; Section 7 summarizes the findings of the research to conclude the article.

3. Concept of the algorithm and proposal of the research

The concept of the whole algorithm is summarized in Fig. 3 by a flowchart and Fig. 4 and Fig. 5 show the image of the calculation step 1 to step 3 and part of step4. Most of the ideas are explained in [10], [11]. The cross-sections and inclinations of tunnels, profiles have meter-order scales in horizontal and height directions. Appendages are centimeter-order scales. Delamination is centimeter-order in areas and millimeter-order in a height direction. To detect small delamination, profiles were removed from raw data. In travel (longitudinal, running) and circumferential (transverse, lane width) directions, profiles were estimated by time series analysis updated by a Kalman filter (Fig. 4, step1) [18], [19].

Hilbert transform was applied to each measurement line to draw an envelope (step2) [20],[21]. Peaks of anomalies were detected by the difference between data and envelopes. The threshold of difference was set 5 mm to detect several millimeter deformations. The algorithm also considers peeling and other types of damages. In this research, only positive peaks were extracted to target delamination. Reference lines were estimated by changing points and extrema. To evaluate areas, detected sections were overplot on a map (step3). Morphology

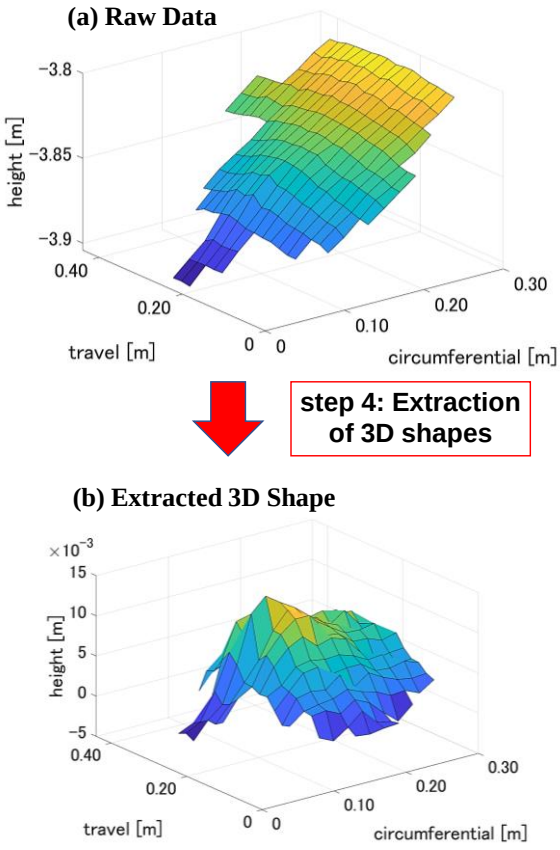

Fig. 5. Extraction of 3D shapes of features by reference planes. (a) Raw data. (b) Extracted 3D shape [11].

transform was applied to smooth areas and remove noises [22],[23].

Reference lines were interpolated by reference planes to extract the 3D shapes of anomalies (Fig.5). 3D features were calculated. The details of the features are explained in section 5. By thresholding feature values, delamination

Table 1
Manual inspection target tunnels and laser data for training and validation of SVM.

Tunnel	Data No.	Location (in Japan)	Construction method	year	Section length (travel by circum.)	No. of delam. (No. of delam. and append. features)
Tunnel 1	No. 1	Nagano pref.	Sheet piling	1975	20 m by 15 m	6 (38, 688)
	No. 2				25 m by 12 m	6 (48, 273)
	No. 3				25 m by 15 m	2 (6, 408)
Tunnel 2	No. 4	Nagano pref.	NATM	1991	22 m by 12 m	0 (0, 138)
Tunnel 3	No. 5	Kanagawa pref.	Sheet piling	1963	60 m by 12 m	2 (78, 484)

is distinguished from appendages. The proposal of this research is related to step 4. In addition to maximum height, area and occupancy, the straightness of anomalies is newly defined to discriminate artificial objects. A classification algorithm based on SVM is applied for automating the detection process. Detected delamination is displayed on a 2D delamination map and 3D quarter view map with its 3D shape.

Fig. 4 (a) displays the raw data of data No. 1. A curved surface corresponds to the ceiling of the tunnel. Profiles, especially cross-sections of tunnels are dominant in tunnel laser data. Fig. 4 (b) shows a map after subtracting estimated profiles from the raw data. Peaks of anomalies were observed. The peaks of cables were continued in a travel direction while lights were local displacements. Even at this step, delamination is not obvious because of the peaks of the appendages. Fig. 4 (c) exhibits circumscribed rectangles of all the detected anomalies after Hilbert transform and Morphology transform. All the features were detected including cables, lights, signs, water guides and delamination.

4. Measurement system and data

4.1. Measurement system

A measurement system shown in Fig. 1 is utilized. A laser sensor irradiates light at each scanning angle and vehicle position. The system adopts two laser sensors to accelerate measurement. Electric signals are converted to optical signals by Laser Diode (LD). Distance is calculated by the phase delay of transmitted and received sinusoidal waves of light. The further details of the principles are out of scope of the research.

Measured distance, called 3D point cloud data, is converted to grid altitude data referring to the GNSS/IMU positioning system. The most important measurement condition is the horizontal resolutions of grid data and corresponding speed of the vehicle. The research adopted a 2 cm resolution. The MMS scans the surfaces of tunnels 10 km/h - 20 km/h to achieve the 2 cm resolution. 50 km/h - 60 km/h the resolution is 5 cm, which is not favorable for the proposed algorithm. Optimization of the measurement conditions remains as future works.

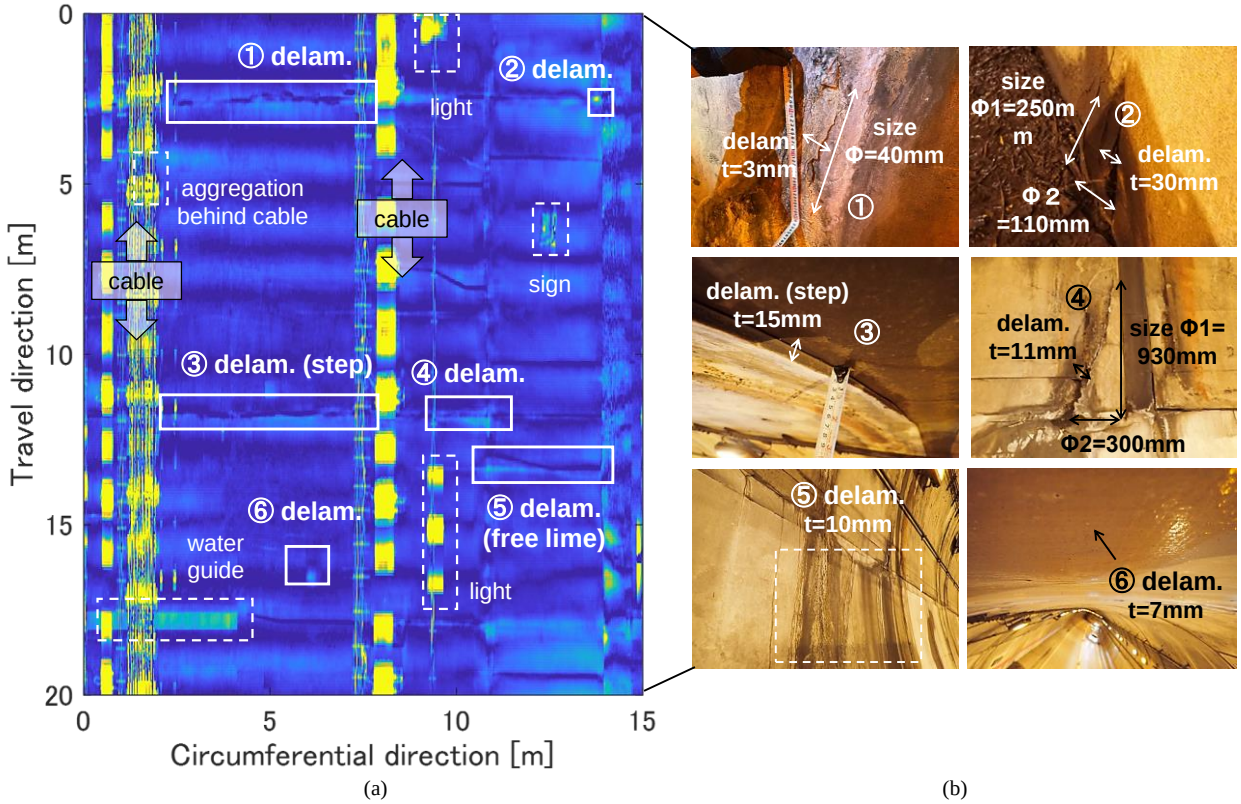

(a) (b)

Fig. 6. Delamination of data No. 1 [11]. (a) Frequency analysis of data and delamination areas detected by manual inspection. Yellow areas are characteristic features emphasized by frequency analysis. (b) Sizes of delamination were measured for references.

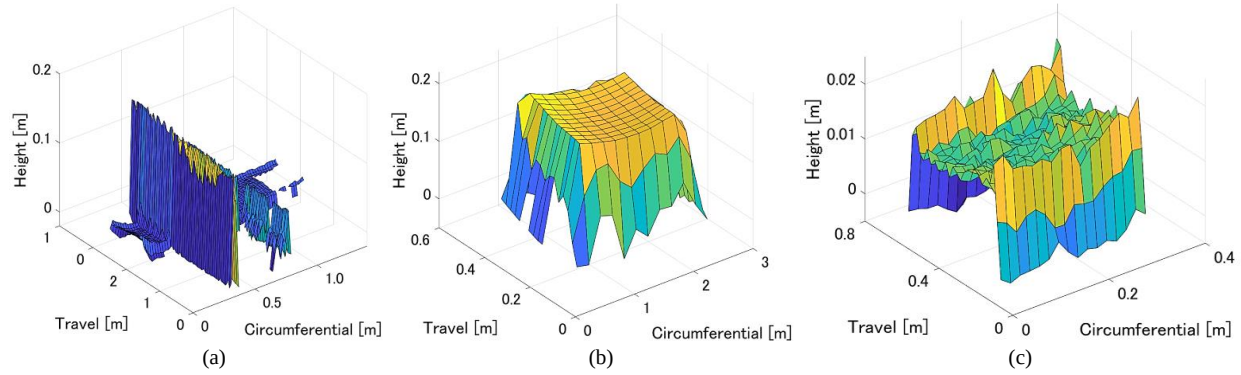

Fig. 7. Extracted 3D shapes. (a) Cable. (b) Light. (c) Water guide. Yellow and blue areas show higher and lower altitude hereafter.

4.2. Data

Table 1 summarizes manual inspection results and measurement data utilized in the research. Three tunnels, five sections from data No. 1 to No. 5 were measured. Sections No. 1 - No. 3 are the same tunnel. Locations are around the capital area of Japan. Tunnel 3 is two hundred kilometers distant from other tunnels. Construction methods and years are also different to demonstrate the applicability of the method. The tunnels are old, ranging from 30 years to 60 years.

Manual inspections were conducted. The total number of delamination is 16. No delamination was detected in data No. 4 except for appendages. Most of the tunnels include multiple areas of delamination, which necessitates dense condition monitoring and assessment. Fig. 6 shows the inspection result of the data No.1. Step-like deformations and delamination caused by free lime are also the targets of the research. Aggregation behind cables cannot be detected in principle and is not the target of the research. To match the positions of manually detected delamination with laser measurement data, features of appendages were utilized. Frequency analysis was applied to emphasize several tens centimeter scale features following the previous research [11],[24]. Frequency analysis is based on short time Fourier transform. The positions of delamination detected by manual inspections were shown referencing characteristic features such as cables, lights and signs (Fig. 5 (a)). Laser measurement points do not exactly correspond to manually detected areas to calculate and validate areas of delamination.

Sizes of damages were also measured for references. Delamination is ambiguous, however, to measure exact maximum height and areas. The performance of the algorithm was evaluated by detected delamination in corresponding areas and falsely detected areas outside the areas as will be explained in section 6. The validation of estimated 3D shapes is not the scope of the research. In the previous research [10], the error was pointed out to be within 20 %.

5. Proposal of 3D features

Fig. 7 shows the examples of extracted 3D features. Fig. 7 (a) - (d) correspond to delamination, cable, light and water guide respectively. Characteristic features are apparent for each type of an object. Considering Fig. 7 (a) - (d), four features were defined. Fig. 8 (a) shows the delamination case. Three features were adopted from the discussions in [11]. The maximum height and areas of features were calculated. These two features are the basic information of the scales of features. The sizes of appendages are larger than delamination while too small features can be ignored as noises. Fig. 8 (b) explains the occupancy of features. Features were projected onto horizontal, circumference-height and travel-height planes, which were perpendicular to vertical, circumferential and travel directions respectively. Circumscribed rectangles

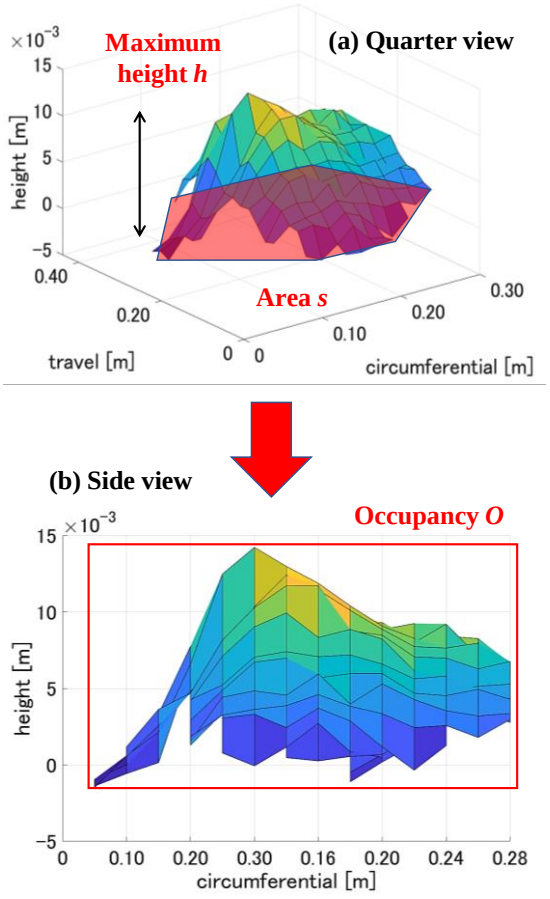

Fig. 8. Extraction of 3D features. (a) Quarter view. (b) Side view. Maximum height, area and occupancy are defined here. Occupancy is estimated from a top view and two side views.

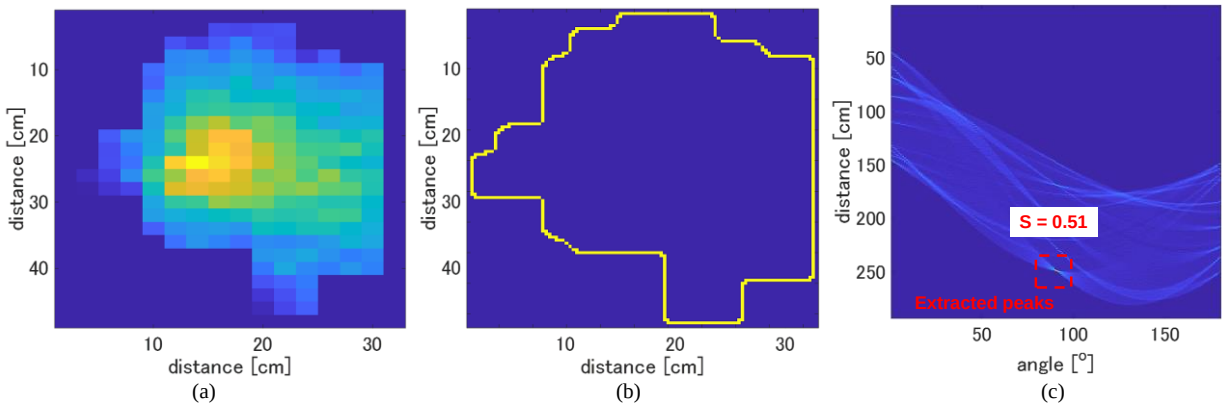

Fig. 9. Extraction of straightness. (a) Area of a feature. The area is the delamination of Fig. 8. (b) Profile of the feature. Profile image is up-sampled. (c) Hough transform of the profile. Five concentrated peaks are extracted to calculate straightness in this case.

were drawn for each projected area. Occupancy is the ratio between the area of the rectangle and projected feature. The concept of occupancy is to simply evaluate the shapes of 3D features. From Fig. 6, cables are wall-like shaped. Lights and signs are box-like shaped. Water guides and repair patches are U-shaped or box-shaped depending on whether features are connected to adjacent features or not. Delamination is convex. The occupancy of box and wall is high, while U-shaped objects are low in a perpendicular direction. The occupancy of a convex is middle on all the projected planes. By thresholding higher and lower occupancy, delamination is detected reducing the detection of appendages and repair-related objects.

Straightness is a simple index proposed in this research. The idea is the profiles of artificial objects are composed of straight lines, while delamination has complicated profiles. Fig. 8 explains the process of evaluating straightness. Fig. 9 (a) displays the area of the delamination of Fig. 8. Fig. 9 (b) shows the profile of the area. Three projected areas can be considered in the same way as occupancy. Therefore, straightness is defined in three directions. Fig. 9 (c) is the Hough transform of the profile of Fig. 9 (b). Too coarse a profile image, e.g. only several pixels by several pixels, will fail in extracting peaks in a Hough space. Therefore, images were up-sampled 10 times in both axes. In the Hough space, each peak corresponds to each straight line. Longer lines are in the image, higher peaks are in the Hough space.

In the Hough space, n highest peaks were detected as lines. $n = 5$ was adopted. The summation I of peak values p_k of extracted n peaks was calculated.

$$I = \sum_{k=1}^{n} p_k \tag{1}$$

The ratio between I and total number of pixels L of the profile is defined as straightness S.

$$S = I/L \tag{2}$$

Longer and more lines are, lager S is. n is the parameter. Too small and too large n will fail in delineating lines. On the other hand, n was confirmed not sensitive to the detection result. It is possibly because relative values of S were compared in SVM and polygons with too many edges did not exist.

Fig. 10 shows the examples of a circle and square to explain the characteristics of straightness. From Fig. 10 (a), S of the square is about 1.1. When all the pixels in an image belong to one of the n straight lines, one pixel increases a peak by one. Consequently, $S \cong 1.0$. Theoretically, in the case of polygons with the number of edges smaller than or equal to n, $S = 1$. Because of the intersections of edges and limited resolutions of images, calculated S is slightly larger than 1.0. Fig. 10 (b) shows a polygon with the infinite number of edges, a circle, indicating $S = 0.3$. S of any profiles is between a polygon and a circle. S of complicated winding and jaggy profiles are small and profiles composed of several straight lines are large. From Fig. 9 (c), $S = 0.5$ in the case of the delamination of Fig. 8. The profile is close to a circle and far from artificial objects.

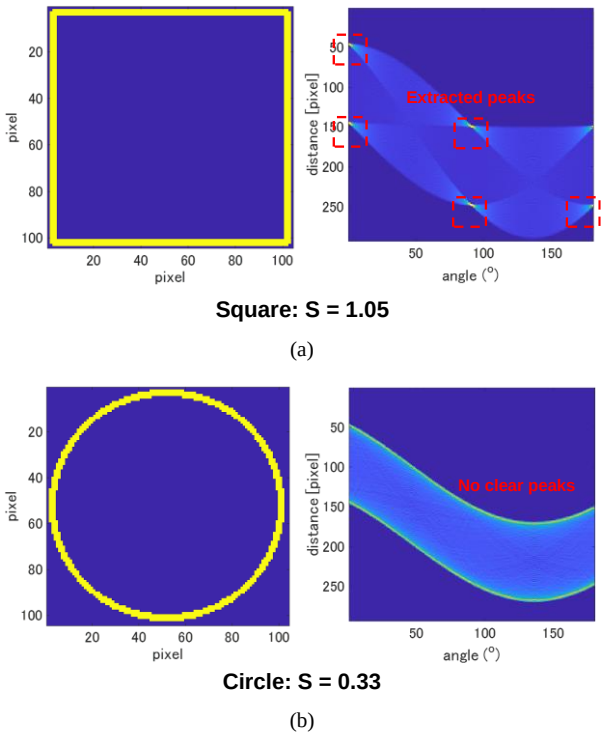

Fig. 10. Examples of straightness of profiles. (a) Square. (b) Circle. Left figure is profile and right one is Hough transform. Calculated straightness is also shown.

One of the most important characteristics of a feature value is scale-invariance. Straightness clearly holds scale-invariance. Straightness holds rotation-invariance. On the other hand, occupancy does not hold rotation-invariance. The successful detection result of delamination indicates most of the analyzed appendages were placed along a travel or circumferential direction, e.g. cables. SVM may automatically construct rotation-invariant features from input feature vectors.

The area and maximum height of a feature are related to the scale of the feature. Occupancy is related to the geometry of the area of the feature. By considering the three directions, 3D geometries are approximately evaluated. However, any polygons with the same areas within circumscribed rectangles will show the same occupancy. Straightness is related to the geometry of the profile of the feature. Considering all the four features, 3D shapes are appropriately evaluated.

Summarizing the above discussions, features about scales, maximum height h and area s, features about the geometries of areas, occupancy in three directions O_{yz}, O_{zx}, O_{xy}, features about the geometries of profiles, straightness in three directions S_{yz}, S_{zx}, S_{xy}, four features

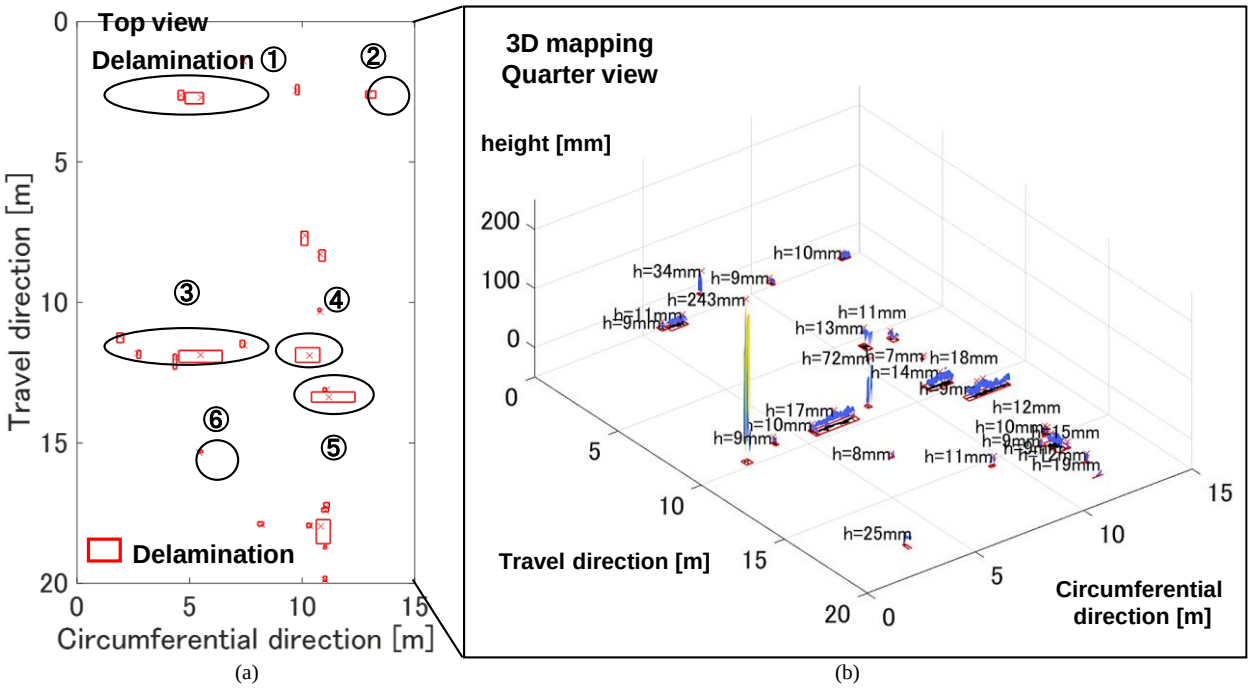

Fig. 11. Detection result of delamination of data No. 1 (a) Top view of 3D mapping result, corresponding to delamination map. (b) Quarter view of 3D mapping result, showing 3D shapes of anomalies. Red cross points represent the highest positions in detected areas with estimated height.

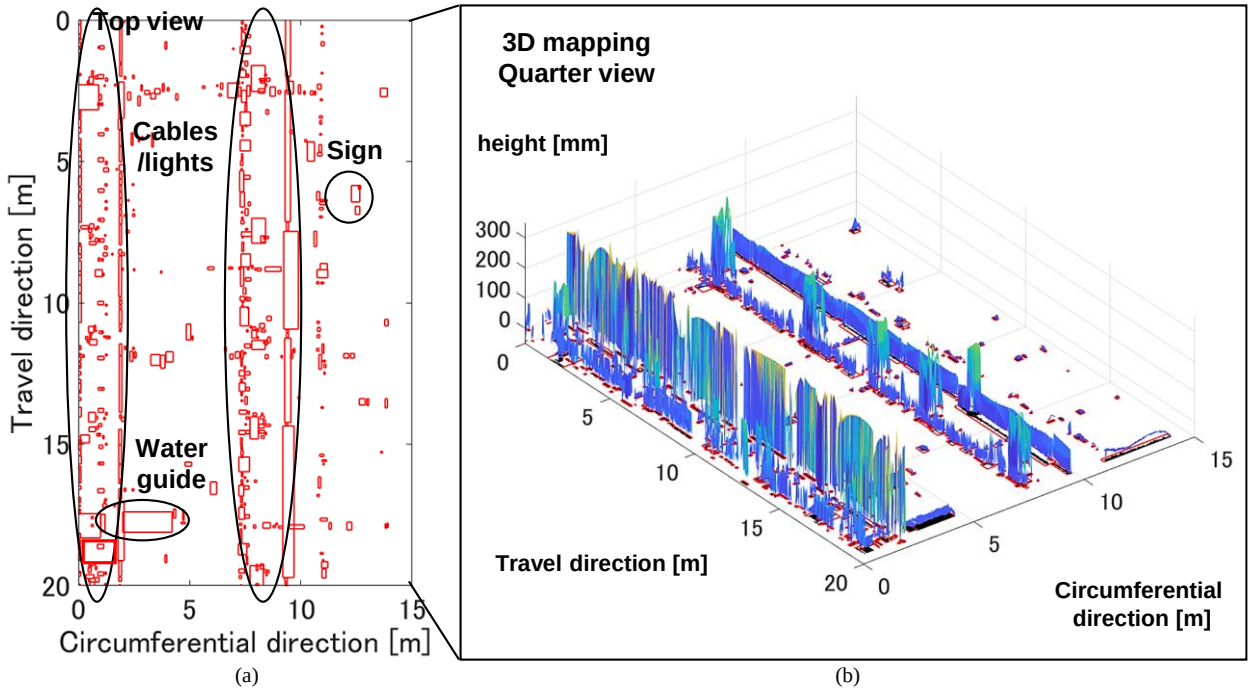

Fig. 12. Detection result of appendages, which are the remaining areas of delamination detection result of Fig. 10. (a) Appendage map. (b) Quarter view of 3D mapping result.

with eight parameters are introduced. An integrated feature vector F is defined below.

$$F = (h, s, O_{yz}, O_{zx}, O_{xy}, S_{yz}, S_{zx}, S_{xy}) \quad (3)$$

Using a feature vector as an input to SVM, a machine learning model was trained to automatically construct the judging criteria of features.

6. Automatic detection by SVM

6.1. Detection results

SVM is one of the simplest classification algorithms with less calculation cost, training data and clear classification criteria among other machine and deep learning methods such as random forests and neural networks [14]-[17], [25]-[26]. Each feature vector is mapped onto a point in a feature space with the same dimension as feature vectors. SVM classifies feature vectors into certain categories by building criteria. It draws optimized linear dividing planes in the feature space by maximizing the distance between the planes and vectors. The vectors which are close to the dividing plane and contribute to the construction of the plane are called support vectors.

In the research, the parameters of SVM were trained by the data shown in Table 1. Data No. 1 of the tunnel 1 was used for validation data. Other four data from No. 2 to No. 5 was used for training data. Areas corresponding to delamination referring to manual inspection results were used as delamination data and others as appendage data. To consider the importance of large area delamination, feature vectors were replicated according to the areas of features. The ratio of the total numbers of detected features between training and validation data is about 3.4 : 1. Cross validation is the most accurate evaluation method. However, because the number and area of delamination vary among the tunnels, it is difficult to divide data No.1 - No. 5 into any other desirable data sets. The data set was produced to hold the generality of the algorithm.

Fig. 11 shows the SVM detection result of data No.1 whose manual inspection result is shown in Fig. 6. The optimization of the SVM model is discussed in the following section. Fig. 11 (a) shows the detected areas of delamination, which was extracted from all the features shown in Fig. 4 (c). Fig. 11 (a) indicates the target delamination No. 1, No. 3 - No. 5 were successfully detected in appropriate positions compared with Fig. 6 (a).

Table 2
Combination of used feature parameters for each SVM model.

SVM model	Used features
No. 1 (Height-Area)	(h, s)
No. 2 (Previous)	$(h, s, O_{yz}, O_{zx}, O_{xy})$
No. 3 (Proposed)	$(h, s, O_{yz}, O_{zx}, O_{xy}, S_{yz})$
No. 4 (All)	$(h, s, O_{yz}, O_{zx}, O_{xy}, S_{yz}, S_{zx}, S_{xy})$

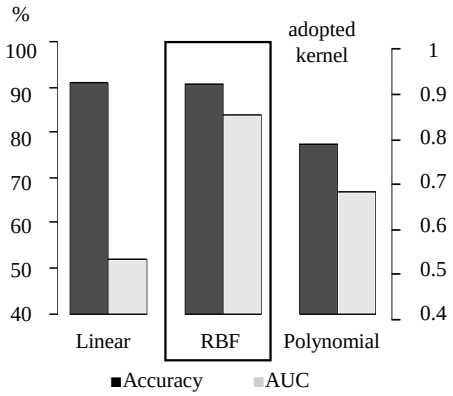

(a)

Fig. 13. Effect of kernel functions on classification accuracy (black) and AUC (gray). Linear is no kernel and polynomial is third order.

The positions of delamination No. 2, No. 6 were shifted, possibly because of the shift in laser data or deformations around the delamination were detected. The total detected areas are 22,540 cm^2 while 16,100 cm^2 is true delamination areas among detected areas. 72 % of detected areas are actual delamination. In the context of deep learning, Intersection over Union (IoU) is the evaluation criterion of matched areas, which is 30 % to 40 % in the case of up-to-date region proposal models [27]-[29]. 72 % is highly precise. By the proposed SVM algorithm, detected regions were localized from 3,000,000 cm^2 to 22,540 cm^2, about 0.8 %. Fig. 11 (b)

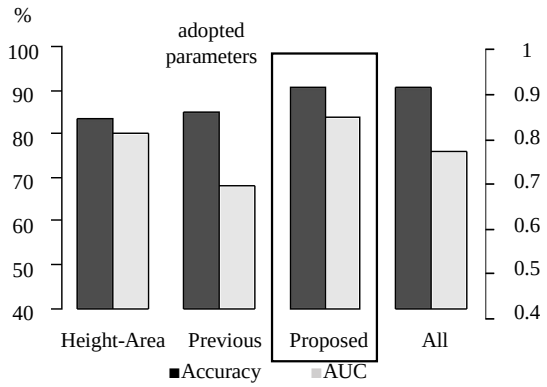

(a)

Fig. 14. Effect of feature parameters on accuracy and AUC.

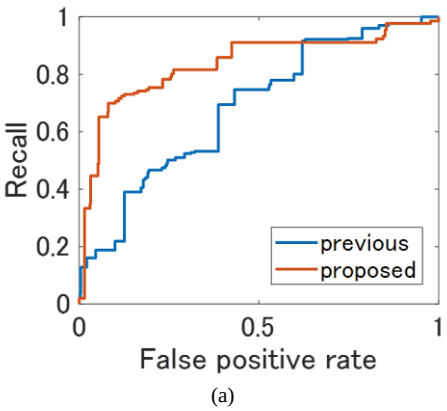

(a)

Fig. 15. Comparison of PR curves of previous (blue) and proposed (red) SVM models.

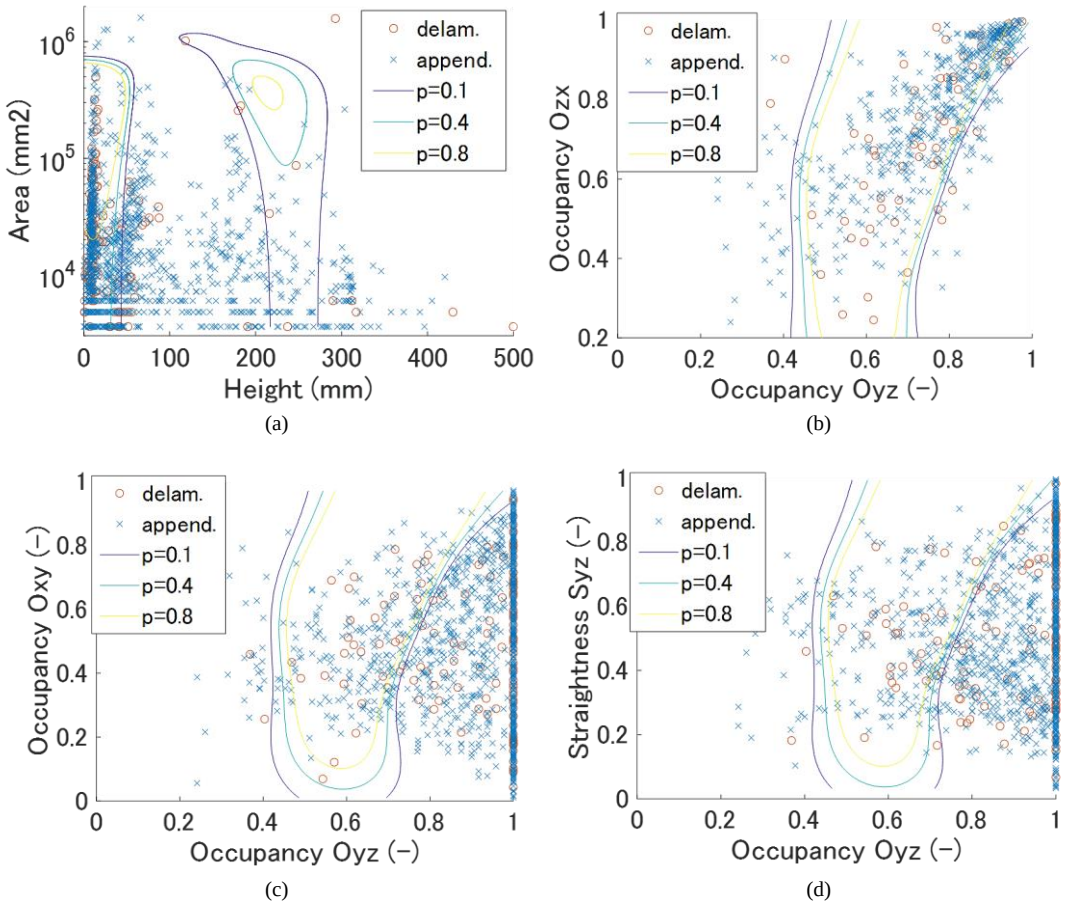

Fig. 16. Scatter plots of feature parameters. Two features were chosen to plot one scatter plot. Red circles are delamination and blue cross points are appendages. Each line shows the contour of probability p = 0.1, 0.4, 0.8, corresponding to the dividing plane of SVM. (a) Height-Area. (b) Occupancy Oyz - Ozx. (c) Occupancy Oyz - Oxy. (d) Occupancy Oyz - Straightness Syz.

shows the quarter view of the estimated 3D shapes to visualize the delamination.

Fig. 12 shows the areas and 3D map of appendages, which remains after removing delamination from all the features. Wall-like features of cables aligned in a travel direction are apparent. Lights between cables, a sign and a water guide were successfully detected as appendages. These features were useful to locate the positions of delamination during repair works and analyze the causes of delamination.

6.2. Parametric study

6.2.1 Kernel function

The important hyper parameter of an SVM model is the choice of a kernel function. Kernel function is a nonlinear conversion applied to input feature vectors, the effect of which is equivalent to drawing nonlinear dividing planes in a feature space. The Kernel function improves the performance of SVM. Fig. 13 shows the comparison of different kernel functions. Polynomial is third order. Accuracy is the rate of correctly classified data among all the data. The data is unbalanced. Area Under the Curve (AUC) of a Precision-Recall (PR) curve is also compared. Accuracy and AUC are not necessarily corresponding with each other [30]. Compared to an ordinally linear SVM, RBF increases the AUC by about 0.3, while the polynomial function decreases accuracy and AUC. The most appropriate kernel function depends on the problem. RBF kernel was adopted.

6.2.2 Feature parameters

Input feature vectors were defined by Eq. (3). To evaluate the effect of introducing parameters, SVM models were compared changing used feature parameters. Table 2 shows the configuration of each SVM model. Model No. 1 (height-area) considers only the scales of anomalies. Model No. 2 (previous) is the model of the previous research introducing occupancy [11]. Model No.3 (proposed) considers straightness of profiles on a horizontal plane. Model No.4 (all) additionally includes straightness in travel and circumferential directions. Accuracy is not compared in the previous research. Fig. 14 compares the accuracy and AUC of each model. The more feature parameters, the larger accuracy is. Considering sizes, occupancy and straightness, the most accurate SVM model is developed. Accuracy of the proposed model was improved by about 6 % compared with the previous model. However, proposed and all models show the same accuracy. Straightness may be redundant; Only considering S_{yz} may be enough. AUC has fluctuation. The profiles of anomalies in travel and circumferential directions are various and may be biased in different tunnel data. Increasing parameters may cause failure in training. Fig. 15 indicates the AUC of the proposed model is improved compared with the previous model.

To visualize the characteristics of obtained SVM criteria, Fig. 16 shows the scatter plots of two parameters and classification criteria constructed by SVM. In Fig. 16,

delamination is red circles and appendages are blue cross points. In SVM training, posterior probability was fitted considering the distance between a dividing plane and feature vectors. The contours of posterior probability $p = 0.1, 0.4, 0.8$ are shown. From Fig. 16 (a) - (d), there are trends in the distribution of feature vectors and curves of probability. From Fig 16 (a), most of the feature vectors are concentrated on small height and areas. From contours, there are strict limit ranges in height. It is suggested there are two groups of small height - small area delamination and large height - large area ones. From Fig. 16 (b) - (d), most of the O_{yz} is concentrated on 1 and from contours there are minimum and maximum O_{yz} limit ranges. This is because delamination is represented by convex peaks showing medium occupancy. There is a slight correlation between O_{yz} and other parameters, which also determines the shapes of contours.

6.2.3 Probability threshold

The probability of delamination p is assigned to each feature vector, which is the only parameter of detection by SVM. Fig. 17 compares the delamination map changing the minimum probability threshold P ($p > P$ holds) from 0.1 to 0.8. Smaller P means safer side evaluation and larger P is vice versa. From Fig. 17 (a) and (b) the whole delamination is detected while false detection increases in the case of $P = 0.1$. On the other hand, from Fig. 16 (c), some delamination is missing in the case of $P = 0.8$. There is a tradeoff between false detections and missing areas. In data No. 1 there are various height and areas of delamination in a 20 m section. Therefore, $P = 0.4$ is valid. In a practical sense, missing delamination may not be favorable. In that case, $P < 0.4$ is appropriate.

7. Conclusions

The automatic and accurate SVM detection algorithm for the delamination on tunnel concrete lining surfaces from laser 3D point cloud data was developed. The algorithm consists of 4 steps: estimation of infrastructure profiles, detection of anomalies by Hilbert transform, localization of areas by Morphology transform, discrimination of delamination from appendages. In the research, step 4 was modified to achieve accurate and automatic detection. The introduction of a novel feature, straightness and automatic detection by SVM were the contributions of the research. Defining the straightness of the profiles of features, artificial objects such as cables and lights were characterized. SVM was trained using data of real tunnel concrete lining surfaces. Including straightness improves accuracy by 6 % and AUC by 0.3 compared with the previous model. A parametric study was conducted to optimize the model and show the most appropriate probability threshold.

For future works, the algorithm can also be applied to the detection of peeling and road potholes. Damages of concrete walls of other types of infrastructures are possible applications. The accurate estimation of tunnel cross-sections from infrastructure profiles extracted in step 1 to monitor tunnel deformations is considered. There is a limitation in measurement vehicle speed. Measuring the same tunnel multiple times may improve the data quality. The inclusion of laser luminance data and optical camera images may increase the accuracy. The developed algorithm is being applied to large-scale tunnel surface data to conduct further detailed regional and statistical analysis.

Acknowledgement

This research was supported by Ministry of Land, Infrastructure, Transport and Tourism (MLIT) “Research and development that contributes to improving the quality of road policies” program (Grant No. 31-6).

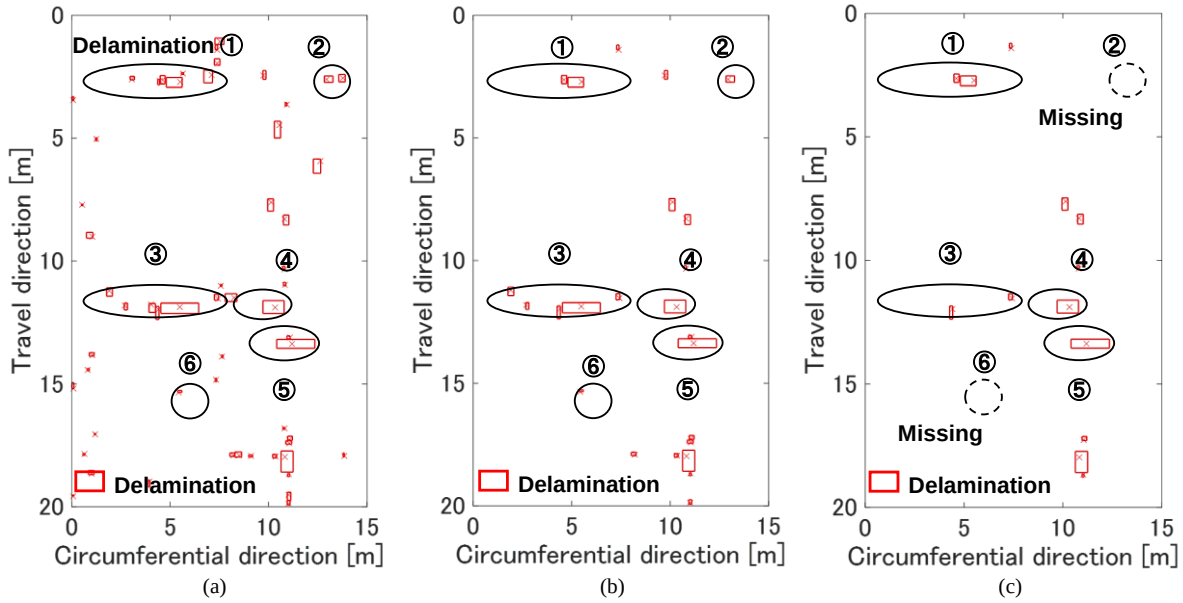

Fig. 17. Delamination maps of the optimized SVM model with different probability threshold P. (a) $P = 0.1$. (b) $P = 0.4$. (c) $P = 0.8$.

Declaration of Competing Interest

None.

References

[1] The World Bank, "Population ages 65 and above," USA. [Online]. Available: https://data.worldbank.org/indicator/SP.POP.65UP.TP.TO.ZS, Accessed on: Oct. 11, 2021.

[2] Ministry of Land, Infrastructure, Transport and Tourism, "Statistics about Road (in Japanese)," Japan. [Online]. Available: https://www.mlit.go.jp/road/soudan/soudan_10.html, Accessed on: Oct. 11, 2021.

[3] Ministry of Land, Infrastructure, Transport and Tourism, "Road tunnel regular inspection manual (in Japanese)," Japan. [Online]. Available: https://www.mlit.go.jp/road/sisaku/yobohozen/tenken/yobo3_1_9.pdf, Accessed on: Jun. 13, 2022.

[4] T. Omar and M. L. Nehdi, "Remote sensing of concrete bridge decks using unmanned aerial vehicle infrared thermography," Automation in Construction, No. 83, pp. 360-371, 2017, DOI: https://doi.org/10.1016/j.autcon.2017.06.024.

[5] S. Blaney and R. Gupta, "Sounding of subsurface concrete defects using frequency response of flexural vibration," Cement and Concrete Composites, No. 92, pp. 155-164, 2018, DOI: https://doi.org/10.1016/j.cemconcomp.2018.06.006.

[6] N. Yasuda, N. Misaki, Y. Shimada and D. Yamaoka, "Detection and characteristics estimation of defects in concrete structures using laser ablation-induced vibration," Tunnelling and Underground Space Technology, Vol. 103, No. 103460, 2020, DOI: https://doi.org/10.1016/j.tust.2020.103460.

[7] Y. Otake, "Non-destructive Infrastructure Testing by Compact Neuron Source," IEEJ Journal, Vol. 139, No. 5, pp. 296-299, 2019, DOI: https://doi.org/10.1541/ieejjournal.139.296.

[8] T. Yamaguchi, T. Mizutani, M. Tarumi and D. Su, "Sensitive damage detection of reinforced concrete bridge slab by "time-variant deconvolution" of SHF-band radar signal," Institute of Electrical and Electric Engineers Transactions of Geoscience and Remote Sensing, Vol. 57, No. 3, 2019. pp. 1478-1488, DOI: https://doi.org/10.1109/TGRS.2018.2866991.

[9] Aero Asahi Corporation, "Roads: mobile mapping system (in Japanese)," Japan. [Online]. Available: https://www.aeroasahi.co.jp/spatialinfo/social_infra/road/, Accessed on: Oct. 11, 2021.

[10] Mizutani, T., Yamaguchi, T., Kudo, T., Yamamoto, K., Ishida, T., Nagata, Y., Kawamura, H., Tokuno, T., Suzuki, K. and Yamaguchi, Y.: Quantitative Evaluation of Peeling and Delamination on Infrastructure Surfaces by Laser Signal and Image Processing of 3D Point Cloud Data, Automation in Construction, No. 133.104023, 2022, DOI: https://doi.org/10.1016/j.autcon.2021.104023.

[11] Mizutani, T., Yamaguchi, T., Kudo, T., Yamamoto, K., Ishida, T., Nagata, Y., Kawamura, H., Tokuno, T., Suzuki, K. and Yamaguchi, Y.: Detection of delamination and peeling on infrastructure surfaces by time series analysis and 3D feature extraction of laser 3D point cloud data, Journal of the Japan Society of Civil Engineers, (under review, to be published).

[12] M. K. Kim, J. C. P. Cheng, H. Sohn and C. C. Chang, "A framework for dimensional and surface quality assessment of precast concrete elements using BIM and 3D laser scanning," Automation in Construction, No. 49, pp. 225-238, 2015, DOI: https://doi.org/10.1016/j.autcon.2014.07.010.

[13] J. S. Yoon, M. Sagong, J. S. Lee and K. S. Lee, "Feature extraction of a concrete tunnel liner from 3D laser scanning data," NDT&E International, No. 42, pp. 97-105, 2009, DOI: https://doi.org/10.1016 /j.ndteint.2008.10.001.

[14] K. Simonyan and A. Zisserman, "Very deep convolutional networks for large-scale image recognition," International Conference on Learning Representations, California, USA, May. 2015, DOI: http://arxiv.org/abs/1409.1556.

[15] C. Szegedy, W. Liu, Y. Jia, P. Sermanet, S. Reed, D. Anguelov, D. Erhan, V. Vanhoucke and A. Rabinovich, "Going deeper with convolutions," Institute of Electrical and Electronics Engineers Conference on Computer Vision and Pattern Recognition, Massachusetts, USA, Jun. 2015, DOI: https://doi.org/10.1109/CVPR.20 15.7298594.

[16] I. Goodfellow, Y. Bengio and A. Courville, "Deep Learning," 1st ed., The MIT Press, Massachusetts, USA, 2016, ISBN: 97802620 35613.

[17] C. M. Bishop, "Pattern Recognition and Machine Learning," 1st ed., Springer, Berlin, Germany, 2006, ISBN: 9780387310732.

[18] M. N. Chatzis, E. N. Chatzi and A. W. Smyth, "An experimental validation of time domain system identifi-cation methods with fusion of heterogeneous data," Earthquake Engineering and Structural Dynamics, Vol. 44, No. 4, pp. 523-547, 2014, DOI: https://doi.org/10.1002/eqe.2528.

[19] D. L. Hall and J. Llinas, "An introduction to multisensor data fusion," Proceedings of the IEEE, Vol. 85, No. 1, pp. 6-23, 1997, DOI: https://doi.org/10.1109/5.554205.

[20] A. V. Oppenheim and R. W. Schafer, "Discrete-Time Signal Processing," 3rd ed., Pearson, London, UK, 2010, ISBN: 9780 131988422.

[21] L. Cohen, "Time-Frequency Analysis," 1st ed., Prentice Hall, New Jersey, USA, 1995, ISBN: 013594532I.

[22] R. M. Haralick, S. R. Sterberg and X. Zhuang, "Image Analysis Using Mathematical Morphology," Institute of Electrical and Electric Engineers Transactions on Pattern Analysis and Machine Intelligence, Vol. PAMI-9, No. 4, pp. 532-550, 1987, DOI: https://doi.org/10.1109/TPAMI.1987.4767941.

[23] R. A. Peters, "A New Algorithm for Image Noise Reduction Using Mathematical Morphology," Institute of Electrical and Electric Engineers Transactions on Image Processing, Vol. 4, No. 5, pp. 554 - 568, 1995, DOI: https://doi.org/10.1109/83.382491.

[24] H. Hirano, T. Mizutani, T. Ishida, S. Annaka, and K. Suzuki, "Evaluation of Local Deterioration of Pavement Surface by Spatial Frequency Analysis based on Short-Time Fourier Transform," Japanese Journal of Pavement Engineering, Vol. 74, No. 3, pp. I_113-I_120, 2018, DOI: https://doi.org/10.2208/jscejpe.74.I_113.

[25] D. F. Llorca, R. Arroyo and M. A. Sotelo, "Vehicle Logo Recognition in Traffic Images using HOG Features and SVM," Institute of Electrical and Electronics Engineers International Conference on Intelligent Transportation Systems, Hague, Netherlands, Oct. 2013, DOI: https://doi/org/10.1109/ITSC.2013.6728559.

[26] Y. Shao and R. S. Lunetta, "Comparison of Support Vector Machine, Neural Network, and CART Algorithms for the Land-cover Classification using Limited Training Data Points," Journal of Photogrammetry and Remote Sensing, No. 70, pp. 78 - 87, 2012, DOI: https://doi.org/10.1016/j.isprsjprs.20 12.04.001.

[27] S. Ren, K. He, R. Girshick and J. Sun, "Faster R-CNN: Towards Real-Time Object Detection with Region Proposal Networks," Institute of Electrical and Electronics Engineers Transactions on Pattern Analysis and Machine Intelligence, Vol. 39, No.6, pp. 1137 - 1149, 2017, DOI: https://arxiv.org/abs/15 06.01497.

[28] W. Liu, D. Anguelov, D. Erhan, C. Szegedy, S. Reed, C. Y. Fu and A. C. Berg, "SSD: Single Shot MultiBox Detector," European Conference on Computer Vision, Amsterdam, Netherland, Oct. 2016, DOI: https://arxiv.org/abs/1512.02325.

[29] J. Redmon, S. Divvala, R. Girshick and A. Farhadi, "You Only Look Once: Unified, Real-Time Object Detection," Institute of Electrical and Electronics Engineers Conference on Computer Vision and Pattern Recognition, Nevada, USA, Jun. 2016, DOI: https://doi.org/10.11 09/CVPR.2016.91.

[30] J. M. Lobo, A. Jimenez-Valverde and R. Real, "AUC: a misleading measure of the performance of predictive distribution model," Global Ecology and Biogeography, No. 17, pp. 145 - 151, 2007, DOI: https://doi.org/10.1111/j.1466-8238.2007.00358.x.